Dual-Scale Porous Electrodes for Solid Oxide Fuel Cells from Polymer Foams**

By *Yuelan Zhang*, *Shaowu Zha*, and *Meilin Liu**

Solid oxide fuel cells (SOFCs) represent one of the cleanest, most efficient, and versatile technologies for chemical-to-electrical energy conversion. It is believed that low-temperature SOFCs have the potential to greatly reduce the cost of the materials required for cell fabrication, in addition to improved reliability, portability, and operational life. However, the interfacial polarization resistances between electrolyte and electrodes increase dramatically as the operating temperature is reduced.[1] Thus, the development of novel electrode materials and/or unique microstructures is one of the critical issues in the development of new generation SOFCs. To date, several new electrode architectures have been developed in order to create durable, effective, and functionally graded electrode structures for intermediate- or low-temperature SOFCs.[2–4] Among these novel electrodes, multiscale porous mixed ionic/electronic conductors (MIECs) are most attractive for SOFCs and catalysis. Since MIECs allow simultaneous transport of both ionic and electronic defects,[5] the use of an MIEC as an electrode may extend the active electrochemical reaction sites from the traditional triple-phase boundaries (TPBs) at the interface between an electronic-conductor electrode and the electrolyte to the entire MIEC/gas interface, which can be orders of magnitude larger than the traditional TPBs. The degree of this extension depends critically on the rate of defect transport through the solid MIEC, the rate of gas transport through the pores, and the catalytic activity of the interfaces. Gas transport through a porous electrode depends largely on the architecture of the electrode. Multiscale porous MIECs are ideally suited for electrode applications: macropores (on the order of micrometers) promote rapid gas transport through the porous electrodes, while nanopores provide high surface areas for gas adsorption/desorption and more catalytically active sites for electrode reactions. However, the creation of such a porous structure is yet to be achieved.

To date, a variety of templating methods that use self-assembly have been used to create structures with submicrometer dimensions. Among them, recent developments using colloidal-crystal templating allow the preparation of ordered macroporous materials that have three-dimensional (3D) ordering of pores with dimensions of tens to thousands of nanometers.[6–12] The use of organic templates to control the structure of inorganic solids has proven very successful, especially in designing porous materials with pore sizes ranging from nano- to micrometers. For example, polymer spheres (PS) have been effectively used as templates to create ordered macroporous oxides, carbon, and polymers with monodisperse, periodic voids in the 0.1–1 μm size range.[10] These synthesis methods rely on filling or coating the void spaces between close-packed spheres with liquid metal alkoxides, resins, or gas-phase precursors and subsequent precursor solidification in situ. Often, the collapse or loss of the 3D porous structure occurs during or after the template removal because of the fragile nature of the materials with wall thicknesses much smaller than the pore size. Although methods for shaping and structuring certain solids into functional objects have been developed and improved to create increasingly more complex features, it is still a challenge to directly apply PS colloidal templating to the synthesis of macroporous MIEC electrode materials. First, the compositions of these electrodes are complicated. For example, a typical composite anode may consist of metallic Ni and $Ce_{0.9}Gd_{0.1}O_{1.95}$ (GDC), while a typical cathode may consist of $Sm_{0.5}Sr_{0.5}CoO_3$ (SSC) and GDC. Thus, it is difficult to obtain the desired stoichiometry from solution containing more than one type of metal precursor using conventional templates. Second, the porous structure must have adequate thermal and mechanical stability during fabrication and operation. Often, it is difficult to retain the macroporous structure of the composite framework, as the template is removed at high temperatures.

In this communication, we report a novel method for preparing multiscale porous MIEC electrode materials using polymer foam as the template, created by evaporating polymer solutions in volatile solvents in a relatively humid environment. Subsequently, a slurry consisted of preformed MIEC nanoparticles was coated on the template. After thermal decomposition of the organic template, the porous MIEC electrode materials remained.

Shown in Figure 1a (insert) are the close-packed synthetic poly(methyl methacrylate) (PMMA) spheres with diameters of about 310 nm prepared by an emulsion polymerization of methyl methacrylate (MMA) in water.[13] The PMMA spheres were suspended in an ethanol/turpentine/xylenes mixture. A film of PMMA foam was readily formed upon spreading several drops of the PMMA suspension onto a yttria-stabilized zirconia (YSZ) substrate in ambient atmosphere (humidity: 65 %). The ethanol, turpentine, and xylenes were evaporated during the subsequent exposure at room temperature, leaving behind a foam-like film, as shown in Figure 1a. The size of the holes is about 1 μm. A slurry containing nanoparticles of MIEC-composite precursors penetrated into the void space within the foam skeleton, coated the surface of the template, and formed the pre-arranged skeleton of the porous composite after solvent volatization, as shown in Figure 1b. Subsequent calcination at 500 °C left the porous MIEC-composite microstructure (Fig. 1c). The regularly and homogenously distributed cellular pores are 0.8–1.5 μm in diameter. The void

[*] Prof. M. Liu, Y. Zhang, Dr. S. Zha
Center for Innovative Fuel Cell and Battery Technologies
School of Materials Science and Engineering
Georgia Institute of Technology
771 Ferst Drive, Atlanta, GA 30332-0245 (USA)
E-mail: meilin.liu@mse.gatech.edu

[**] This work was supported by DOE-NETL under grant No. DE-FC26-02NT41572.

DOI: 10.1002/adma.200400466

ADVANCED MATERIALS

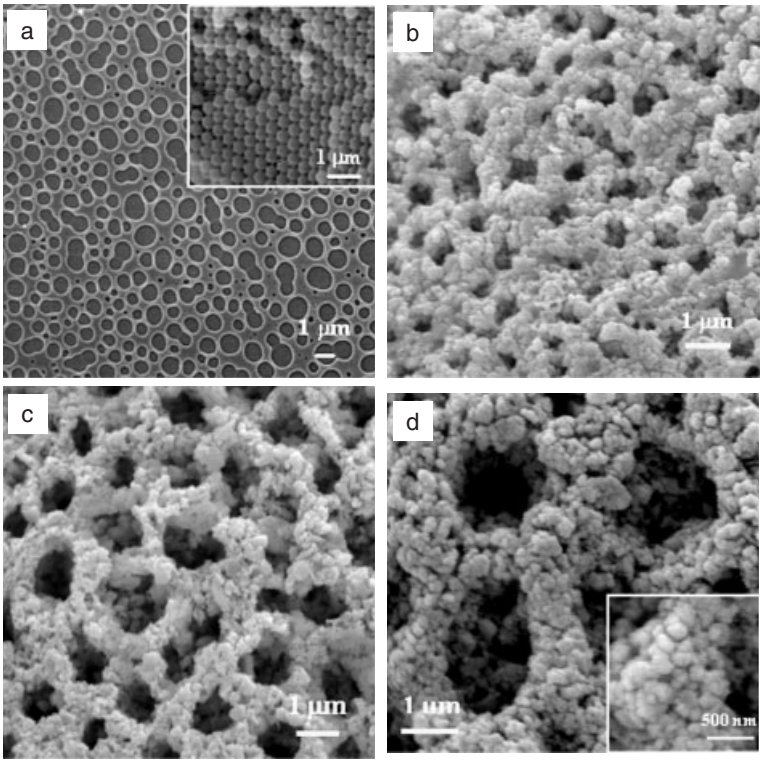

Figure 1. Scanning electron microscopy (SEM) images of a) foamy PMMA structure (the insert shows close-packed PMMA spheres); b) as-prepared structure of foamy PMMA after infiltration with SSC–GDC slurry; and c,d) porous SSC–GDC electrode materials after firing at 550 °C for 5 h (the insert shows an enlargement of the wall composed of MIEC nanoparticles).

spaces were interconnected in three dimensions via walls approximately 0.5–1 μm in thickness. Figure 1d is an enlarged view of Figure 1c. Further investigation of the microscopic features of the wall shown in Figure 1d revealed that the pore walls were built from nanoparticles with an average diameter of about 100 nm. The voids between these particles form a continuous and nanoporous wall structure. In this way, dual porosity (macro- and mesopores) is created.

The Brunauer–Emmett–Teller (BET) surface area and the pore volume were estimated using N_2-adsorption measurements on samples degassed for 4 h at 300 °C (Fig. 2a). The specific surface area of the porous structure as determined using the BET method is about 19 $m^2 g^{-1}$. Shown in Figure 2b is the pore size distribution, as calculated using Barrett–Joyner–Halenda (BJH) theory from the N_2-desorption data. The two peaks centered at around 2.5 nm and 35 nm indicate that the walls of the cells were also mesoporous and a combined meso-/macroporous structure was created.

The vapor-condensation patterns that form on cold surfaces are known as "breath figures".[14] Beysens et al. have studied the phenomena of water-droplet condensation on cold solid surfaces.[15] Also, it is well-known that evaporation of volatile organic liquids can lead to condensation of water droplets in the submicrometer size range.[16,17] Solvent evaporation decreases the air–liquid interfacial temperature. If the temperature falls below the dew point, water droplets condense on the surface. Ethanol, turpentine, and xylene are relatively volatile.

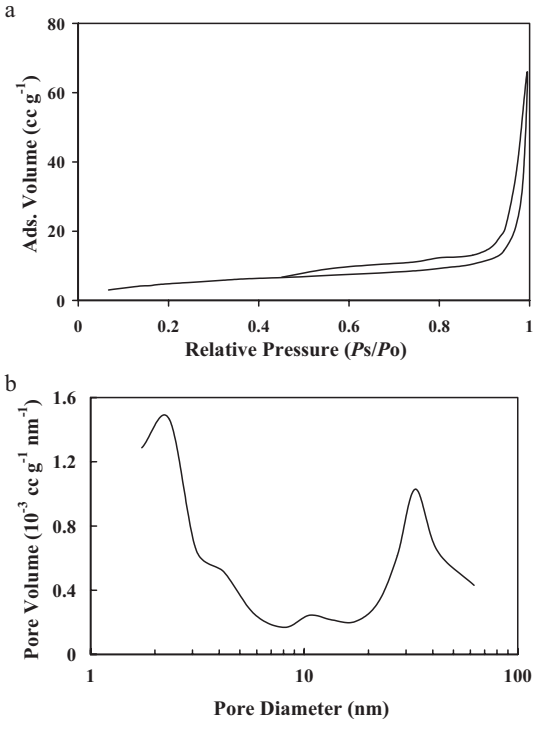

Figure 2. a) Nitrogen adsorption–desorption isotherms for porous GDC–SSC materials calcined in air at 800 °C for 2 h. b) The corresponding BJH pore size distribution.

The high vapor pressure of the solvents drives solvent evaporation and rapidly cools the surface. This cooling leads to the condensation of water droplets on the evaporating surface, which then grow and interact. The interaction between droplets, coupled with convective currents in the evaporating solvents, drive the self-assembly of the packing of the water droplets.[15–19] When the solvents are less dense than water, the porous array will propagate through the film,[16] producing a 3D array. The obtained morphologies present very regular and homogenous pore structures. Instead, the morphologies obtained from templating of single colloidal-crystal spheres have characteristically monodisperse and periodic pore structures. Hence, in this study, it is this polymeric superstructure that acts as template, instead of the direct templating of single polymer spheres.

Figure 3 shows scanning electron microscopy (SEM) images of a dual-scale porous electrode, composed of a continuous network of SSC and 30 wt.-% GDC MIEC composite, after the removal of the template by firing at 800 °C. The porous array of submicrometer-sized holes extends over a range of thousands of micrometers on the substrate (Fig. 3a). As shown in Figure 3b, the electrode consisted of regularly distributed cellular pores with 1 μm diameters. The interconnected walls are approximately 0.5–1 μm thick. The primary particles of the composite are about 100 nm in diameter. It is noted that the wall of the network is nanoporous due to the burn-off of the organic binder in the slurry, which is an ideal structure for a SOFC electrode, and superior to the structure shown in Figure 3c formed without a template. The micrometer-diameter interconnected pores facilitate fast gas diffusion and mass transport, while the nanoporous walls consisting of much smaller grains of MIEC greatly enhance the rate of interfacial reactions.

Changes of the templated morphologies can occur in conventional templating approaches, as significant shrinkage[6,7] and crystal growth are often observed.[7] To date, only one paper has reported the successful synthesis of ordered macroporous SSC.[2] In the present method, the firing temperature has a smaller effect on the pore size and particle size. The pore sizes produced by a firing temperature of 800 °C are almost the same as at 550 °C, which is about 1 μm. Similarly, the wall thicknesses are about 0.5–1 μm at both temperatures. This is because, first, there is less room for the precursor to shrink, as the polymer spheres are being removed because the precursor is made of a solid suspension instead of a liquid solution. Second, there is much less shrinkage due to the particle growth because the SSC and GDC powders are pre-heat-treated at high temperature; as shown Figure 3b (insert), there is no sign of significant grain growth. Third, the wall is comparatively thick and strong enough to support the whole structure after removal of template. Compared to conventional polymer-sphere templating processes, thicker pore walls with mechanically more stable materials were obtained due to the templating of the polymeric superstructure instead of single spheres.

Furthermore, the desired stoichiometric composition had been assured before the infiltration. Figure 4a shows the X-ray diffraction (XRD) patterns of prepared MIECs, implying that the films are composed of the desired SSC and GDC phases.

Shown in Figure 5a are the impedance spectra of one cell with the configuration of SSC-GDC/$(Bi_2O_3)_{0.75}(Y_2O_3)_{0.25}$/Pt measured at 700 °C and 800 °C under open-circuit conditions.

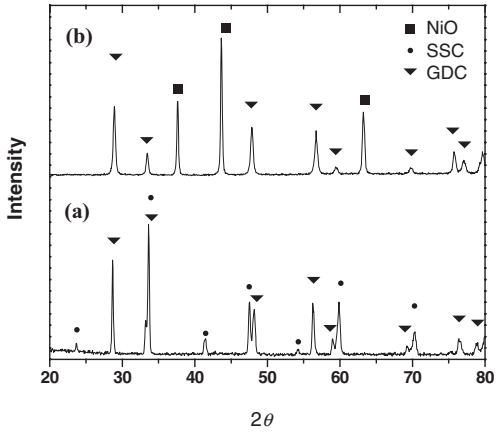

Figure 4. X-ray diffraction patterns of a) a composite cathode (SSC and 30 wt.-% GDC), and b) a composite anode (NiO and 35 wt.-% GDC).

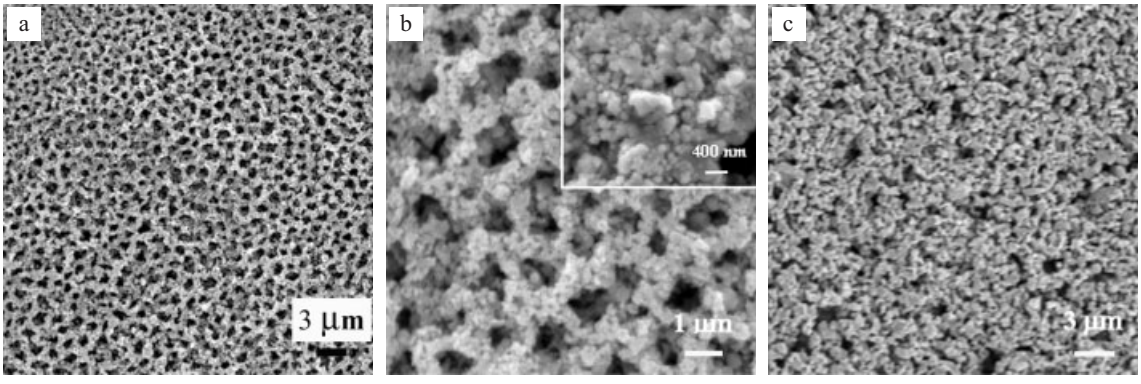

Figure 3. SEM micrographs of a,b) an interconnected porous SSC–GDC MIEC cathode fired at 800 °C for 2 h (the insert in (b) shows the nanostructure of the porous wall area), and c) SSC–GDC MIEC cathode prepared by slurry coating without a template.

ADVANCED MATERIALS

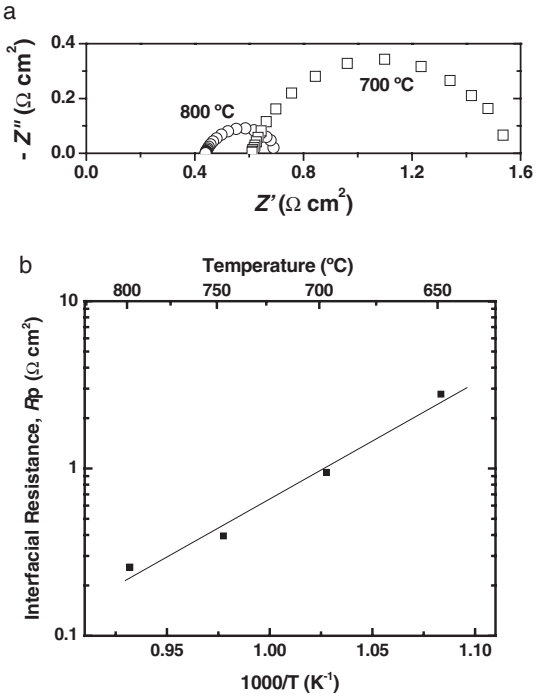

Figure 5. a) Impedance spectra for a cell with configuration of SSC–GDC/$(Bi_2O_3)_{0.75}(Y_2O_3)_{0.25}$/Pt, where Z' and Z'' represent the real and the imaginary part of the impedance (in Ω cm^2), respectively. b) The cathodic polarization resistances, R_p, of the interface between the porous GDC–SSC electrode and the dense $(Bi_2O_3)_{1.75}(Y_2O_3)_{0.25}$ electrolyte as determined from impedance spectra acquired at different temperatures.

Figure 5b presents the Arrhenius plots of SSC–GDC cathode/electrolyte interfacial polarization resistance. At 750 °C, the cathodic interfacial resistance is as low as 0.39 Ω cm^2, implying that the porous cathode is promising for the use in intermediate-temperature SOFCs.

The methodology of this templating process appears to be readily extendable to other electrode materials, as long as the size of the precursor particles is in the nanometer range. For example, a porous anode consisting of NiO and GDC was obtained using the same process, followed by firing at 800 °C (Fig. 6). The NiO–GDC composite was verified by the XRD pattern (shown in Fig. 4b). Large regions of regular and homogeneous holes with diameters of about 1 μm were formed under the same conditions. The wall is also porous and about 1 μm thick, while the average primary particle size is about 100 nm.

In summary, the preparation and characterization of novel, regular, and homogeneous MIEC materials with dual porosities for SOFC electrodes have been described. Foam-like thin-film templates are formed by water condensation from a relatively humid environment induced by evaporation of volatile solvents. The template was used to direct the porous structure of MIEC materials. After removal of the organic template by calcination, the resulting SSC–GDC and NiO–GDC composite electrodes retained their macroscopic shapes. It provides a promising way to synthesize dual-scale porous electrodes for solid oxide fuel cells.

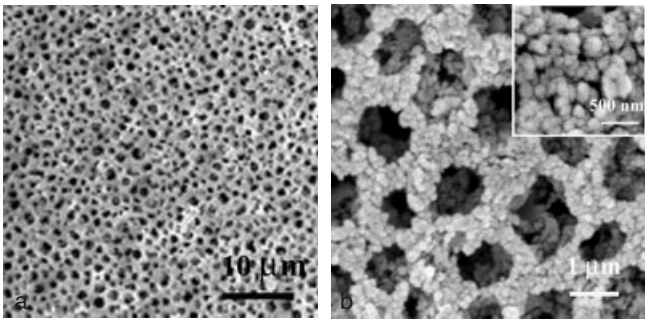

Figure 6. a,b) SEM images of a dual-scale porous NiO–GDC anode film fired at 800 °C for 2 h. The insert in (b) shows the nanostructure of the porous wall.

Experimental

Materials: Methyl methacrylate (99.9 %) monomer and 2,2′-azobis(2-methylpropionamidine) dihydrochloride initiator were purchased from Aldrich. One precursor for multiscale porous mixed ionic/electronic conductor (MIEC) electrodes, $(NH_4)_2Ce(NO_3)_6$ (99.99 %), was purchased from Aldrich, while $Gd(NO_3)_3{\cdot}6\,H_2O$ (99.9 %), $Ni(NO_3)_2{\cdot}6\,H_2O$, $Sm(NO_3)_3{\cdot}6\,H_2O$ (99.9 %), $Sr(NO_3)_2$ (99.0 %), and $Co(NO_3)_2{\cdot}6\,H_2O$ (98.5 %) were purchased from Alfa Aesar. Glycine, acetone, ethanol, and xylenes were purchased from Fisher, and turpentine from Heraeus. All materials were used as received.

Synthesis of Poly(methyl methacrylate) (PMMA) Colloids: Monodisperse PMMA spheres were synthesized using an surfactant-free emulsion procedure which was previously described in the literature [13]. Typically, 15 wt.-% methyl methacrylate and 84.88 wt.-% distilled water were placed into a three-neck round-bottomed flask. The system was maintained at 80 °C with moderate stirring for 30 min to attain temperature equilibrium. Then, a specific amount of the initiator, 0.12 wt.-% 2,2′-azobis(2-methylpropionamidine) dihydrochloride, was added. The reaction was maintained at 80 °C for another 3 h, and then cooled to room temperature. The close-packed PMMA spheres were obtained by centrifugation and dried under ambient conditions for one week.

Preparation of MIEC Materials: Nanocrystal $Ce_{0.9}Gd_{0.1}O_2$ (GDC) powder, $Sm_{0.5}Sr_{0.5}CoO_3$ (SSC) powder, and NiO powders were prepared using a glycine–nitrate process (GNP), which is described in detail elsewhere [20–22]. The stoichiometric amounts of precursors $(NH_4)_2Ce(NO_3)_6$ and $Gd(NO_3)_3{\cdot}6\,H_2O$ were dissolved in 40 mL distilled water to form an 0.5 M aqueous solution, to which solid glycine was then added. The molar ratio of NO_3^- to glycine was maintained at 2. The resulting solution was then heated to evaporate the excess solvent on a hot plate, and the residual viscous resin transformed to a dark-brownish foam. When heated further, it ignited, yielding a voluminous, yellow, sponge-like ash. NiO and SSC powders were prepared with a similar procedure. The as-prepared GDC, SSC, and NiO ashes were subsequently fired at 600 °C, 800 °C, and 850 °C, respectively.

Preparation of Slurries: Proportional amounts with the weight ratio 1:1:2 of SSC and GDC powder/V006 binder/acetone were mixed together by ball-milling for at least 24 h. The ratio of electronic conductor SSC to ionic conductor GDC powders was 7:3 by weight. The slurry for the anode consisting of 65 wt.-% NiO and 35 % GDC was prepared in a similar manner [21,22].

Film Formation: Synthetic close-packed PMMA spheres were crushed into powders which were subsequently dispersed in an 80:10:10 (by volume) ethanol/turpentine/xylenes mixture. The concentration of spheres ranged from 5 to 9 wt.-%. The PMMA suspension was dropped and spread on the surface of the yttria-stabilized zirconia (YSZ) or GDC pellet. Then, the polymer film was dried at ambient at-

mosphere for two hours (humidity:65 %). The slurry was then diluted by ethanol and drop-cast onto the top of the template using small syringes. As the solvent permeated the interstices of the polymer foams, the nanocrystals of the composites in the slurry also permeated into the interstices and coated the foams. The coated sample was maintained under an ambient atmosphere for 1 h, then was heated and held at 60 °C for 2 h, and finally underwent thermal decomposition of the organic template. The samples were calcined in air, first at 350 °C for 3 h, and then fired at 550 °C for 5 h with a heating rate of 2 °C min^{-1}. Some of the samples were subsequently fired at 800 °C for 2 h. The PMMA foam and binder decomposed during calcination, yielding dual-scale porous MIEC thin films.

Characterization: X-ray powder diffraction (XRD) patterns were acquired on a Philips PW-1800 X-ray diffractometer with Cu Kα radiation. N_2-adsorption measurements were performed at 77 K with a Micromeritics ASAP 2000 system. The samples were degassed at 300 °C for 4 h. Scanning electron microscopy (SEM) images were obtained using a Hitachi S-800 scanning electron microscope. Impedance measurements were performed at temperature range of 650–800 °C in a frequency range of 0.01 Hz to 100 KHz with a Signal Recovery lock-in amplifier (model 5210) and an EG&G potentiostat/galvanostat (model 273 A) interfaced with a computer. The cell configuration was SSC–GDC/$(Bi_2O_3)_{0.75}(Y_2O_3)_{0.25}$/Pt.

Received: March 27, 2004
Final version: September 25, 2004

[1] C. Xia, M. Liu, *Adv. Mater.* **2002**, *14*, 521.
[2] F. L. Chen, C. R. Xia, M. L. Liu, *Chem. Lett.* **2001**, *10*, 1032.
[3] S. Zha, Y. L. Zhang, M. L. Liu, *Solid State Ionics* **2005**, *176*, 25.
[4] C. R. Xia, Y. L. Zhang, M. L. Liu, *Electrochem. Solid-State Lett.* **2003**, *6*, A290.
[5] M. Liu, *J. Electrochem. Soc.* **1997**, *144*, 1813.
[6] A. Stein, *Microporous Mesoporous Mater.* **2001**, *44–45*, 227.
[7] B. T. Holland, C. F. Blanford, A. Stein, *Science* **1998**, *281*, 538.
[8] O. D. Velev, T. A. Jede, R. F. Lobo, A. M. Lenhoff, *Nature* **1997**, *389*, 447.
[9] O. D. Velev, E. W. Kaler, *Adv. Mater.* **2000**, *12*, 531.
[10] H. Yan, C. F. Blanford, B. T. Holland, W. H. Smyrl, A. Stein, *Chem. Mater.* **2000**, *12*, 1134.
[11] Y. A. Vlasov, N. Yao, D. J. Norris, *Adv. Mater.* **1999**, *11*, 165.
[12] Y. Xia, B. Gates, Y. Yin, Y. Lu, *Adv. Mater.* **2000**, *12*, 693.
[13] D. Zou, S. Ma, R. Guan, M. Park, L. Sun, J. J. Aklonis, R. Salovey, *J. Polym. Sci., Part A: Polym. Chem.* **1992**, *30*, 137.
[14] T. J. Baker, *Philos. Mag. (1798–1977)* **1922**, *44*, 752.
[15] D. Beysens, C. M. Knobler, *Phys. Rev. Lett.* **1986**, *57*, 1433.
[16] A. Steyer, P. Guenoun, D. Beysens, C. M. Knobler, *Phys. Rev. B: Condens. Matter Mater. Phys.* **1990**, *42*, 1086.
[17] M. Srinivasarao, D. Collings, A. Philips, S. Patel, *Science* **2001**, *292*, 79.
[18] A. V. Limaye, R. D. Narhe, A. M. Dhote, S. B. Ogale, *Phys. Rev. Lett.* **1996**, *76*, 3762.
[19] P. S. Shah, M. B. Sigman, Jr., C. A. Stowell, K. T. Lim, K. P. Johnston, B. A. Korgel, *Adv. Mater.* **2003**, *15*, 971.
[20] L. A. Chick, L. R. Pederson, G. D. Maupin, J. L. Bates, L. E. Thomas, G. J. Exarhos, *Mater. Lett.* **1990**, *10*, 6.
[21] S. W. Zha, J. G. Cheng, Y. Liu, G. Y. Meng, *Solid State Ionics* **2003**, *156*, 197.
[22] S. W. Zha, A. Moore, H. Abernathy, M. L. Liu, *J. Electrochem. Soc.* **2004**, *151*, A1128.

Enhanced Ferroelectric Properties of Nitrogen-Doped $Bi_4Ti_3O_{12}$ Thin Films**

By *Hiroshi Irie*,* *Hiroyuki Saito*, *Shin-ichi Ohkoshi*, and *Kazuhito Hashimoto*

Ferroelectrics are excellent candidates for data-storage applications in digital-memory systems. Many groups have enthusiastically investigated the ferroelectrics for applications in ferroelectric random-access memories (FeRAMs).[1–12] $SrBi_2Ta_2O_9$ (SBT), which is a bismuth layer-structured oxide (BLSO), has several advantages, such as being fatigue-free up to 10^{12} cycles and requiring low operation voltage.[3–5] However, SBT has the disadvantage of a small remnant polarization, P_r (15 μC cm^{-2}). A promising alternative material to SBT is $Bi_4Ti_3O_{12}$ (BIT, also a kind of BLSO) due to its large spontaneous polarization (50 μC cm^{-2}, along the *a*- or *b*-axis),[6,7] but thin films and ceramics of BIT have a large leakage current due to defects and a large coercive field, E_c. The leakage behavior interferes with the poling process by an applied field, and the large coercive field requires a large operation voltage, which limits the practicality of these devices. The defects also act as the pinning sites of domain motions, which leads to a small P_r of 7.5 μC cm^{-2}.[8–12] Some research has focused on enhancing P_r and/or reducing the leakage current of BIT in the thin film and ceramic forms. For example, a thin film of lanthanum-substituted BIT ($Bi_{3.25}La_{0.75}Ti_3O_{12}$) was reported to have a relatively high P_r of 12 μC cm^{-2} and a good fatigue resistance.[13] Noguchi et al. controlled defects by incorporating vanadium or tungsten into titanium sites and by introducing excess bismuth, which resulted in a very large P_r and low current leakage. However, they also reported a large, simultaneous increase in E_c.[14,15] To date, an increase in P_r and a decrease in E_c seem to be mutually exclusive.[16] Previous studies have focused on incorporating other elements into the metal sites in the BLSOs and in other ferroelectric materials. PZT [$Pb(Zr,Ti)O_3$] is a representative material with zirconium incorporated into the titanium sites. This paper examines the incorporation of nitrogen at oxygen sites in BIT, resulting in an increase of P_r (17.7 μC cm^{-2}), a decrease of E_c (105 kV cm^{-2}), and an enhancement of the fatigue properties ($> 10^9$ cycles).

Tabata and co-workers, and Katayama-Yoshida and co-workers, both successfully fabricated p-type ZnO by nitrogen doping.[17–20] ZnO is essentially an n-type semiconductor due to its deviation from stoichiometry, i.e., it possesses oxygen

[*] Dr. H. Irie, H. Saito, Prof. S. Ohkoshi, Prof. K. Hashimoto
Research Center for Advanced Science and Technology
The University of Tokyo
4-6-1 Komaba, Meguro-ku, Tokyo 153-8904 (Japan)
E-mail: irie-hrs@light.t.u-tokyo.ac.jp

[**] This work was supported by CREST, Japan Science and Technology Agency (JST).

 DOI: 10.1002/adma.200400957